Sensor Placement in District Heating Networks Using Frequency-Domain Gramians

Sibeijn, Max; Pequito, Sergio; Boskos, Dimitris; Khosravi, Mohammad

DOI
10.1109/LCSYS.2025.3580027

Publication date
2025

Document Version
Final published version

Published in
IEEE Control Systems Letters

Sensor Placement in District Heating Networks Using Frequency-Domain Gramians

Max Sibeijn, *Graduate Student Member, IEEE*, Sérgio Pequito, *Senior Member, IEEE*, Dimitris Boskos, *Member, IEEE*, and Mohammad Khosravi, *Member, IEEE*

***Abstract*—District heating networks (DHNs) are essential in providing efficient heating services to urban areas through networked pipes. The performance of these systems critically depends on the strategic placement of thermal storage buffers (actuators) and temperature sensors throughout the network. Due to the inherent slow dynamics of thermal transport, these systems exhibit significant delays and periodic behaviors that necessitate time-varying analysis approaches. This letter presents a frequency-domain framework for optimal actuator and sensor placement in DHNs, focusing on metrics derived from frequential Gramians. We provide rigorous analysis of two key metrics, namely the trace and log-determinant of the frequential Gramian, establishing submodularity properties and performance guarantees for greedy selection algorithms. Our theoretical framework naturally handles both the periodic nature of DHNs and their slow transients, outperforming standard approaches in estimation accuracy.**

***Index Terms*—Time-varying systems, energy systems, sensor placement, submodular optimization.**

I. Introduction

A FUNDAMENTAL challenge in district heating network (DHN) operation is the strategic placement of thermal storage buffers (actuators) and temperature sensors throughout the network to control it [1], [2]. The slow dynamics of thermal transport, with delays of hours from generation to consumption [3], [4], complicate this task. While prior work explored optimal storage [5] and sensor placement [6], challenges persist. Poor actuator placement delays responses and wastes energy, while suboptimal sensors hinder thermal state estimation [7].

Traditional actuator and sensor placement methods rely on controllability and observability metrics from linear system theory [8], [9], using Gramian analysis to assess energy requirements for state control and measurement. However, these approaches are insufficiently equipped to handle the slow periodic dynamics present in DHNs, characterized by daily demand cycles [10]. Beyond classic LTI-based techniques, several approaches were developed for nonlinear or time-varying systems, including empirical Gramians [11], data-driven methods [12], and time-domain analysis for time-varying systems [13]. While powerful in specific contexts, these methods are not necessarily suited for DHNs: empirical Gramians and time-domain approaches require intensive computation for large-scale networks, and data-driven approaches raise concerns regarding the collection and quality of training data and the design of basis functions.

Recent advances in frequency-domain analysis, particularly frequential Gramians, provide an efficient framework for studying DHN dynamics. These methods offer both theoretical and computational advantages over time-domain approaches [14], naturally capturing the system's periodicity and slow thermal transients.

This letter presents a frequency-domain framework for optimal sensor placement in DHNs, focusing on observability metrics derived from frequential Gramians. We provide rigorous analysis of two key metrics: the trace and log-determinant of the frequential observability Gramian, establishing submodularity properties and performance guarantees for greedy selection algorithms. Our theoretical framework naturally handles both the periodic nature of DHN dynamics and their slow transients, offering computational advantages over traditional time-domain approaches. Furthermore, we demonstrate how these metrics can be efficiently computed using truncated Fourier representations.

II. Optimal Sensor Placement Problem for District Heating Networks

In this section, we formalize the minimal sensor placement problem for DHNs. To this end, we first model the DHN using transport equations and conservation principles, then provide a precise mathematical formulation of the optimization problem.

A. District Heating Network Dynamics

1) Network Structure: We model a DHN as a strongly connected directed graph $\mathcal{G} = (\mathcal{N}, \mathcal{E})$ with a set of nodes

Received 17 March 2025; revised 10 May 2025; accepted 27 May 2025. Date of publication 16 June 2025; date of current version 15 July 2025. This work was supported by the Local Inclusive Future Energy (LIFE) City Project, funded by the Ministry of Economic Affairs and Climate and by the Ministry of the Interior and Kingdom Relations of the Netherlands under Grant MOOI32019. Recommended by Senior Editor A. Loria. *(Corresponding author: Max Sibeijn.)*

Max Sibeijn, Dimitris Boskos, and Mohammad Khosravi are with the Delft Center for Systems and Control, Delft University of Technology, 2628 CD Delft, The Netherlands (e-mail: m.w.sibeijn@tudelft.nl; d.boskos@tudelft.nl; mohammad.khosravi@tudelft.nl).

Sérgio Pequito is with the Department of Electrical and Computer Engineering, Instituto Superior Técnico, University of Lisbon, 1049-001 Lisbon, Portugal (e-mail: sergio.pequito@tecnico.ulisboa.pt).

Digital Object Identifier 10.1109/LCSYS.2025.3580027

$\mathcal{N}$ that represent junctions in the DHN, which are connected by edges $\mathcal{E} \subseteq \mathcal{N} \times \mathcal{N}$, representing pipelines that may be fitted with pumps, valves, or heat exchangers. Note that strong connectivity of $\mathcal{G}$ ensures no mass exits the system. The *incidence matrix* $E \in \mathbb{R}^{|\mathcal{N}|\times|\mathcal{E}|}$ of $\mathcal{G}$ describes the edge-to-node relationship, i.e., for any $(i,k) \in \{1,2,\ldots,|\mathcal{N}|\} \times \{1,2,\ldots,|\mathcal{E}|\}$, we have $E_{ik} = -1$ if the k^{th} edge *exits* node i, $E_{ik} = 1$ if the k^{th} edge *enters* node i, and $E_{ik} = 0$ otherwise.

2) Transport Dynamics: The temporal evolution of temperature distributions within pipeline systems is characterized by

$$\partial_t T(x,t) + v(t)\partial_x T(x,t) + \zeta\,(T(x,t) - T_{\text{amb}}) = 0, \tag{1}$$

where $T(x,t)$ represents the temperature distribution, $v(t)$ is the flow velocity, t is time, x is the spatial coordinate, T_{amb} represents the ambient temperature and ζ is a heat loss coefficient. A finite-dimensional representation of the pipeline dynamics is obtained by applying spatial discretization using the upwind scheme to (1) for each pipe segment $e \in \mathcal{E}$, i.e.,

$$\partial_t T_j^e(t) = -v_e(t)\frac{T_j^e(t) - T_{j-1}^e(t)}{\Delta x} - \zeta_e\big(T_j^e(t) - T_{\text{amb}}\big), \tag{2}$$

for $j = 1,\ldots,m_e$. Here, T_j^e denotes the temperature in segment j of edge e. The term v_e is the flow velocity in edge e, while ζ_e is the heat loss coefficient for edge e. The total number of discretization segments for edge e is given by m_e and Δx represents the spatial discretization step size.

3) Node Constraints: At each network node, the conservation of mass principle combined with the incompressibility assumption requires that the total volumetric flow rate entering the node equals the total volumetric flow rate exiting the node. To formalize this, we define for each node $n \in \mathcal{N}$ two sets: $\mathcal{E}_{\to n} = \{e \in \mathcal{E} : e \text{ enters } n\}$, containing all edges entering node n, and $\mathcal{E}_{n\to} = \{e \in \mathcal{E} : e \text{ exits } n\}$, comprising all edges exiting node n. The mass conservation principle at each node is then expressed through the flow balance equation given by $\sum_{e\in\mathcal{E}_{\to n}} q_e(t) = \sum_{e\in\mathcal{E}_{n\to}} q_e(t)$, where $q_e(t) = \phi_e v_e(t)$ represents the flow rate in pipe e, with ϕ_e denoting the cross-section of pipe. Additionally, energy balance at each node is enforced through a mixing rule that relates the node's exit temperature to the temperatures of incoming flows, i.e.,

$$T_n(t) = \frac{\sum_{e\in\mathcal{E}_{\to n}} q_e(t) T_{m_e}^e(t)}{\sum_{e\in\mathcal{E}_{\to n}} q_e(t)}. \tag{3}$$

The temperature of any edge leaving a node equals that node's temperature, yielding $T_0^e(t) = T_n(t)$, $\forall\, n \in \mathcal{N}$, $\forall\, e \in \mathcal{E}_{n\to}$.

4) Coupled Network Equations: The coupled network dynamics combine edge dynamics from the discretized thermal energy equation (2) with the mentioned nodal constraints. For each edge $e \in \mathcal{E}$, we define the edge variable $x_e(t) = [T_j^e(t) - T_{\text{amb}}\,]_{j=0}^{m_e}$, representing temperature deviations from ambient. The complete state vector $x(t) \in \mathbb{R}^m = [x_e(t)\,]_{e\in\mathcal{E}}$ concatenates all edge states across the network. The dynamical system is described by the periodic continuous-time dynamics

$$\begin{aligned} \dot{x}(t) &= A(t)x(t), \quad A(t+T) = A(t), \\ A(t) &= \frac{1}{2\Delta x} E\,V(t)(|E|_o - E)^\top - \operatorname{diag}(\zeta_i)_{i\in\mathbb{N}_m}, \end{aligned} \tag{4}$$

with $V(t) = \operatorname{diag}(v_e(t))_{e\in\mathcal{E}}$, $\mathbb{N}_m := \{1,\ldots,m\}$, and $|\cdot|_o$ denoting the element-wise absolute value operator. The periodicity of $A(t)$ emerges from cyclical flow patterns $V(t)$ driven by consistent consumer demand cycles [10].

B. Problem Statement

Consider the following T-periodic linear system, representing the DHN dynamics described for any $t \in \mathbb{R}$ as

$$\begin{aligned} \dot{x}(t) &= A(t)x(t) + B_{\mathcal{I}}u(t), \quad A(t+T) = A(t), \\ y(t) &= C_{\mathcal{J}}x(t), \end{aligned} \tag{5}$$

where $x(t) \in \mathbb{R}^m$, $u(t) \in \mathbb{R}^{|\mathcal{I}|}$, $y(t) \in \mathbb{R}^{|\mathcal{J}|}$, and $A(\cdot)$ is continuous. Furthermore, $B_{\mathcal{I}}$ and $C_{\mathcal{J}}$ are structured matrices where $B_{\mathcal{I}} = I_m(\mathcal{I})$ and $C_{\mathcal{J}} = I_m(\mathcal{J})$. Here, I_m is the $m \times m$ identity matrix, with $\mathcal{I}$ and $\mathcal{J}$ indicating the positions of columns and rows corresponding to dedicated actuators and sensors that control and measure single nodes, respectively. While we restrict the analysis in this letter to the placement of sensors, the results readily extend to the placement of actuators by invoking arguments similar to duality between controllability and observability in LTI systems. Furthermore, one should note that the arguments and discussion in this letter can be generalized to any systems satisfying (5).

Our goal is to identify a minimal subset of sensors $\mathcal{J} \subseteq \{1,2,\ldots,m\}$ ensuring sufficient sensing capabilities. To quantify sensing performance, we introduce a performance metric $\rho : 2^{\mathbb{N}_m} \mapsto \mathbb{R}$ based on the *time-averaged frequential observability Gramian* $\Lambda_{\mathcal{J}}$, defined rigorously in Section III, which generalizes the classical observability Gramian to periodically time-varying linear systems as a measure of observability. We employ two established metrics: the *geometric mean energy*, defined as $\rho(\mathcal{J}) = \log\det(\Lambda_{\mathcal{J}}^{-1})$, and the *average energy*, defined as $\rho(\mathcal{J}) = \operatorname{tr}(\Lambda_{\mathcal{J}}^{-1})$, quantifying the effort required for state reconstruction across all state dimensions. Our objective is to solve the following optimization problem:

$$\begin{aligned} \min_{\mathcal{J}\subseteq\{1,2,\ldots,m\}} \quad & |\mathcal{J}| \\ \text{s.t.} \quad & \rho(\mathcal{J}) \le K \end{aligned} \tag{6}$$

where K is a positive threshold constant. For the metrics under consideration, this formulation represents an instance of well-known NP-hard problems [15].

III. Time-Averaged Frequential Gramian

In this section, we establish frequential Gramian theory, computation, and properties for submodular optimization.

The frequential Gramian derives from Fourier coefficients that encode structural information across the frequency modes of the periodic system. For a T-periodic matrix $A(\cdot)$, Floquet's theorem yields a T-periodic coordinate change $z(t) = Q(t)x(t)$ in which the uncontrolled dynamics take the time-invariant form $\dot{z}(t) = Fz(t)$, where F is constant. The eigenvalues of F are the so-called Floquet exponents, which determine the stability of perturbations of periodic orbits. We henceforth assume F has no eigenvalue on the imaginary axis.

For the Floquet transformed system, there exist T-periodic Gramians that can be computed at discrete time points

as the outer product of T-periodic frequency-domain factors [14, Proposition 2]. When these Gramians are mapped from Floquet coordinates back to physical coordinates, the resulting Gramians can be constructed using analogous periodic frequency-domain factors. Specifically, the frequential Gramian in physical coordinates, indicating the frequential energy content with respect to time lag t, is defined as [14, Eqn. 21]:

$$G_{\mathrm{f}}(t,\mathcal{J}) = \frac{1}{2\pi}\int_{-\infty}^{\infty} \Psi(\gamma,t,\mathcal{J})\Psi(\gamma,t,\mathcal{J})^{\mathsf{H}}\ \mathrm{d}\,\gamma, \tag{7}$$

where G_{f} is well-defined (see Lemma 1), and $\Psi : \mathbb{R}\times[0,T)\times 2^{\mathbb{N}_m} \mapsto \mathbb{C}^{m\times m}$ are the frequency-domain factors given by

$$\Psi(\gamma,t,\mathcal{J}) = \sum_{k\in\mathbb{Z}} \Psi_k(\gamma,\mathcal{J})\,\mathrm{e}^{\mathrm{i}\,k\omega t}, \quad t\in[0,T), \tag{8}$$

where $\omega = \frac{2\pi}{T}$ is the *fundamental frequency*.

In what follows, we provide the Fourier coefficients $\Psi_k(\gamma,\mathcal{J})$ following [14, Proposition 3], where the reader can find further details on their construction. Let $(A_k)_{k\in\mathbb{Z}}$ be the Fourier coefficients of $A(\cdot)$, and define $\mathbf{R}_k = (-\mathrm{i}\,k\omega I_m + A_0)$. Given the corresponding Fourier basis for $A(\cdot)$, we define the infinite-dimensional matrix $\mathbf{T} = [\mathbf{T}_{ij}]_{i,j=-\infty}^{\infty}$, consisting of the block matrices $\mathbf{T}_{ij}\in\mathbb{C}^{m\times m}$ defined as

$$\mathbf{T}_{ij} = \begin{cases} \mathbf{R}_i, & \text{if } i=j,\\ A_{i-j}, & \text{if } i\neq j. \end{cases} \tag{9}$$

Subsequently, for any $\gamma\in\mathbb{R}$, define $\mathcal{H}(\gamma) = (\mathrm{i}\,\gamma I_\infty - \mathbf{T})^{-1}$. It is worth noting that $\mathcal{H}(\gamma)$ is called the *harmonic resolvent operator*, mapping harmonic components between inputs and outputs, i.e., $[\mathcal{H}(\gamma)]_{k,\ell}$ represents the m by m block of $\mathcal{H}(\gamma)$ mapping the inputs at frequency $\gamma+\ell\omega$ to the outputs at frequency $\gamma+k\omega$, for any $k,\ell\in\mathbb{Z}$. Accordingly, for any $k\in\mathbb{Z}$, $\gamma\in\mathbb{R}$, and $\mathcal{J}\subseteq\mathbb{N}_m$, the function $\Psi_k : \mathbb{R}\times 2^{\mathbb{N}_m}\to\mathbb{C}^{m\times m}$ is defined analogously to [14, eq. 31]; however, $C_{\mathcal{J}}$ is treated as time-invariant, so only the $j=0$ component is non-zero:

$$\Psi_k(\gamma,\mathcal{J}) = \left[\mathcal{H}(\gamma)^{\mathsf{H}}\right]_{k,0} C_{\mathcal{J}}^{\mathsf{H}}. \tag{10}$$

Thus, we have a closed-form expression for the Fourier coefficients, which subsequently enables the computationally efficient approximation of the frequential Gramian in (7).

In this letter, we are interested in optimal sensor placement to maximize the average temporal sensing performance for the DHN. Therefore, we define the *time-averaged frequential Gramian* $\Lambda_{\mathcal{J}} : 2^{\mathbb{N}_m}\to\mathbb{R}^{m\times m}$ as

$$\Lambda_{\mathcal{J}} = \frac{1}{T}\int_0^T G_{\mathrm{f}}(\tau,\mathcal{J})\ \mathrm{d}\,\tau. \tag{11}$$

Proposition 1: For a given set of sensors $\mathcal{J}\subseteq\mathbb{N}_m$ and a system with period T, the time-averaged frequential Gramian $\Lambda_{\mathcal{J}}\in\mathbb{R}^{m\times m}$ satisfies

$$\Lambda_{\mathcal{J}} = \frac{1}{2\pi}\int_{-\infty}^{\infty}\sum_{k\in\mathbb{Z}} \Psi_k(\gamma,\mathcal{J})\Psi_k(\gamma,\mathcal{J})^{\mathsf{H}}\ \mathrm{d}\,\gamma. \tag{12}$$

Proof: Using Tonelli's theorem, we can exchange the order of integration to get

$$\Lambda_{\mathcal{J}} = \frac{1}{2\pi T}\int_{-\infty}^{\infty}\int_0^T \Psi(\gamma,\tau,\mathcal{J})\Psi(\gamma,\tau,\mathcal{J})^{\mathsf{H}}\ \mathrm{d}\,\tau\ \mathrm{d}\,\gamma. \tag{13}$$

Subsequently, substituting in the Fourier series representation of $\Psi(\gamma,\tau,\mathcal{J})$ from (8), the inner integral becomes

$$\begin{aligned}\int_0^T &\Psi(\gamma,\tau,\mathcal{J})\Psi(\gamma,\tau,\mathcal{J})^{\mathsf{H}}\ \mathrm{d}\,\tau\\ &= \int_0^T \sum_{k\in\mathbb{Z}}\sum_{l\in\mathbb{Z}} \Psi_k(\gamma,\mathcal{J})\Psi_l(\gamma,\mathcal{J})^{\mathsf{H}}\ \mathrm{e}^{\mathrm{i}(k-l)\omega\tau}\ \mathrm{d}\,\tau\\ &= T\sum_{k\in\mathbb{Z}} \Psi_k(\gamma,\mathcal{J})\Psi_k(\gamma,\mathcal{J})^{\mathsf{H}},\end{aligned} \tag{14}$$

where the last equality follows from Fubini's theorem and the orthogonality of complex exponentials, i.e., the integral $\int_0^T \mathrm{e}^{\mathrm{i}(k-l)\omega\tau}$ equals T if $k=l$, and 0 if $k\neq l$. Therefore, the time-averaged frequential Gramian takes the form given in (12), which completes the proof. ∎

Interpretation: For each γ, the operator $\Psi_k(\gamma,\mathcal{J})$ characterises how the k^{th} Floquet harmonic of the state manifests in the measured output channels indexed by $\mathcal{J}$. The Hermitian product $\Psi_k(\gamma,\mathcal{J})\,\Psi_k(\gamma,\mathcal{J})^{\mathsf{H}}$ therefore quantifies the observable energy of that harmonic. Integrating over γ and summing over $k\in\mathbb{Z}$ collect these contributions into $\Lambda_{\mathcal{J}}$.

Remark 1: The temporal dependency of $G_{\mathrm{f}}(t,\mathcal{J})$ on t stems from the system's convergence to a periodic trajectory. For any t, the Gramian already contains full period information. While $G_{\mathrm{f}}(t,\mathcal{J})$ could be used to determine optimal active sensors, tracking the period for sensor scheduling presents practical implementation challenges difficult to overcome in real-world applications. Hence, we focus on the time-averaged frequential Gramian for sensor placement.

A. Approximate Gramian Computation

The formulation in (12) reveals that the time-averaged frequential Gramian decomposes into a sum of contributions from each frequency mode. Nonetheless, exact computation of $\Lambda_{\mathcal{J}}$ is challenging as it requires inverting an infinite-dimensional matrix and evaluating an improper integral. We introduce an approximation to make this computation tractable and tight, namely by truncation of higher-order Fourier modes and discretization of the frequency domain. In particular, we consider a uniformly sampled set of frequencies $\Gamma := \{\gamma_1,\ldots,\gamma_L\}$, and a truncation order r of the Fourier series of $A(\cdot)$, i.e., $A_r(t) := \sum_{k=-r}^{r} A_k\,\mathrm{e}^{\mathrm{i}\,k\omega t}$. This consequently reduces $\mathbf{T}$ to a finite matrix of dimension $(2r+1)m\times(2r+1)m$, with $\widehat{\mathcal{H}}_r(\gamma)$ representing the corresponding truncation of $\mathcal{H}(\gamma)$. We formalize the mentioned results below.

Proposition 2: Given Γ and r, for the time-averaged frequential Gramian $\Lambda_{\mathcal{J}}$, we have

$$\Lambda_{\mathcal{J}} = \frac{1}{\pi}\sum_{\gamma_l\in\Gamma}\xi_l \sum_{k=-r}^{r}\widehat{\Psi}_k(\gamma_l,\mathcal{J})\widehat{\Psi}_k(\gamma_l,\mathcal{J})^{\mathsf{H}} + \mathcal{R}_{\mathcal{J}}(r,L), \tag{15}$$

where ξ_l are quadrature coefficients,

$$\widehat{\Psi}_k(\gamma_l,\mathcal{J}) = \left[\widehat{\mathcal{H}}_r(\gamma_l)^{\mathsf{H}}\right]_{k,0} C_{\mathcal{J}}^{\mathsf{H}}$$

are approximations of the Fourier coefficients $\Psi_k(\gamma_l,\mathcal{J})$ at frequency γ_l, and the residual term $\mathcal{R}_{\mathcal{J}}(r,L)$ goes to zero as $r\to\infty$ and $L\to\infty$.

Proof: The convergence of the residual term to zero is directly implied from the uniform convergence of the Fourier

series of Ψ over compact subsets of the domain of γ and the integrability of $G_{\mathrm{f}}(t)$. ■

Corollary 1: The time-averaged frequential Gramian can be efficiently approximated and computed by determining $\Psi_k(\gamma_l, \mathcal{J})$ only over a narrow band of positive frequencies.

Proof: For the efficient approximation of the truncated Gramian, i.e., the first term in right-hand side of (15), we exploit the fact that for any $\gamma \in \mathbb{R}$, there exists an $\ell \in \mathbb{Z}$ such that $\alpha = \gamma - \ell\omega \in (-\omega/2, \omega/2]$, and

$$\Psi_k(\gamma, \mathcal{J}) = \left[\mathcal{H}(\alpha)^{\mathsf{H}}\right]_{k,\ell} C_{\mathcal{J}}^{\mathsf{H}}. \tag{16}$$

Additionally, since the dynamics are real-valued, their Fourier coefficients are symmetric and we get from (10) and the definition of $\mathbf{T}$ that $\Psi_k(-\gamma, \mathcal{J}) = \mathrm{conj}(\Psi_k(\gamma, \mathcal{J}))$. These properties reduce the frequency evaluation range to $\alpha \in (-\omega/2, \omega/2] \cap [0, \infty) = [0, \omega/2]$. For each shift index $\ell \in \{-r, \ldots, 0, \ldots, r\}$, define

$$\mathbf{C}_{\mathcal{J}}^{(\ell)} = \mathbf{e}_{\ell+r+1} \otimes C_{\mathcal{J}}^{\mathsf{H}} \tag{17}$$

where $\mathbf{e}_{\ell+r+1}$ is the $(\ell + r + 1)$-th unit basis vector in $\mathbb{R}^{2r+1}$. We find $\Psi_{\mathcal{J},\alpha_l}^{(\ell)} \in \mathbb{R}^{(2r+1)m \times |\mathcal{J}|}$ by solving the linear system

$$(\mathrm{i}\,\alpha_l I_m - \mathbf{T})^{\mathsf{H}}\, \Psi_{\mathcal{J},\alpha_l}^{(\ell)} = \mathbf{C}_{\mathcal{J}}^{(\ell)}, \tag{18}$$

for $\alpha_l \in [0, \omega/2]$ and $l \in \{1, \ldots, L\}$. We can retrieve the approximate value of $\Psi_k(\gamma_l, \mathcal{J})$ at $\gamma_l = \alpha_l + c\omega$ by taking the k^{th} block of $\Psi_{\mathcal{J},\alpha_l}^{(\ell)}$, i.e., we have

$$\widehat{\Psi}_k(\gamma_l, \mathcal{J}) = \left[\Psi_{\mathcal{J},\alpha_l}^{(\ell)}\right]_k = \left[\widehat{\mathcal{H}}_r(\alpha_l)^{\mathsf{H}}\right]_{k,\ell} C_{\mathcal{J}}^{\mathsf{H}}. \tag{19}$$

Applying numerical quadrature to (12) with these approximated coefficients and exploiting the established symmetry properties yields (15), which completes the proof. ■

B. Properties of Frequential Gramians

We state two important results on the properties of the time-averaged frequential Gramian.

Lemma 1: Suppose none of the Floquet exponents of the system lie on the imaginary axis. Then, for any $\mathcal{J} \subseteq \mathbb{N}_m$, the time-averaged frequential Gramian $\Lambda_{\mathcal{J}}$, introduced in (11), is well-defined and positive semi-definite, i.e., $\Lambda_{\mathcal{J}} \succeq 0$. Moreover, it is additive, i.e., for any $\mathcal{J}_1, \mathcal{J}_2 \subseteq \mathbb{N}_m$, we have

$$\Lambda_{\mathcal{J}_1 \cup \mathcal{J}_2} = \Lambda_{\mathcal{J}_1} + \Lambda_{\mathcal{J}_2 \setminus \mathcal{J}_1}. \tag{20}$$

Proof: We prove each property separately.

Well-definedness: For both stable and unstable time-periodic systems, the frequential Gramian $G_{\mathrm{f}}(t)$ is well-defined since none of the Floquet exponents of the system lie on the imaginary axis. This follows from the fact that each Floquet-transformed Fourier coefficient of the Gramian satisfies a Sylvester equation, as exemplified in [14, Proposition 1]. It follows that $\Lambda_{\mathcal{J}}$ is also well-defined.

Positive Semi-definiteness: Let $x \in \mathbb{R}^n$. Then

$$\begin{aligned} x^\top \Lambda_{\mathcal{J}} x &= \frac{1}{2\pi} \int_{-\infty}^{\infty} \sum_{k \in \mathbb{Z}} x^\top \Psi_k(\gamma, \mathcal{J}) \Psi_k(\gamma, \mathcal{J})^{\mathsf{H}} x \, \mathrm{d}\,\gamma \\ &= \frac{1}{2\pi} \int_{-\infty}^{\infty} \sum_{k \in \mathbb{Z}} \| \Psi_k(\gamma, \mathcal{J})^{\mathsf{H}} x \|^2 \, \mathrm{d}\,\gamma \geq 0. \end{aligned} \tag{21}$$

Since the above expression is non-negative for any $x \in \mathbb{R}^n$, we have $\Lambda_{\mathcal{J}} \succeq 0$ for all $\mathcal{J} \subseteq \mathbb{N}_m$.

Additivity: Consider two sets $\mathcal{J}_1, \mathcal{J}_2 \subseteq \mathbb{N}_m$. By the structure of $C_{\mathcal{J}}$, we can write

$$\begin{aligned} \Psi_k(\gamma, \mathcal{J}_1 \cup \mathcal{J}_2) &= \left[\mathcal{H}(\gamma)^{\mathsf{H}}\right]_{k,0} C_{\mathcal{J}_1 \cup \mathcal{J}_2}^{\mathsf{H}} \\ &= \left[\mathcal{H}(\gamma)^{\mathsf{H}}\right]_{k,0} \begin{bmatrix} C_{\mathcal{J}_1}^{\mathsf{H}} & C_{\mathcal{J}_2 \setminus \mathcal{J}_1}^{\mathsf{H}} \end{bmatrix} \\ &= \begin{bmatrix} \Psi_k(\gamma, \mathcal{J}_1) & \Psi_k(\gamma, \mathcal{J}_2 \setminus \mathcal{J}_1) \end{bmatrix}. \end{aligned} \tag{22}$$

Substituting this expression into the definition of the frequential Gramian and using the linearity of integration, we obtain $\Lambda_{\mathcal{J}_1 \cup \mathcal{J}_2} = \Lambda_{\mathcal{J}_1} + \Lambda_{\mathcal{J}_2 \setminus \mathcal{J}_1}$, which completes the proof. ■

Lemma 2: For LTI systems, the time-averaged frequential observability Gramian from (12) reduces to the standard observability Gramian.

Proof: Consider a stable LTI system with $A(t) = A$ for all $t \in \mathbb{R}$. For brevity, we write C instead of $C_{\mathcal{J}}$. The standard observability Gramian W_o satisfies $A^\top W_o + W_o A = -C^\top C$. For LTI systems, (10) yields a single nonzero Fourier coefficient $\Psi_0(\gamma, \mathcal{J}) = (\mathrm{i}\,\gamma I_m - A^\top)^{-1} C^\top$ since off-diagonal blocks of $\mathbf{T}$ vanish. Substituting into (12), we obtain the time-averaged frequential observability Gramian for LTI systems:

$$\Lambda_{\mathcal{J}}^{\mathrm{LTI}} = \frac{1}{2\pi} \int_{-\infty}^{\infty} \left(\mathrm{i}\,\gamma I_m - A^\top\right)^{-1} C^\top C (-\mathrm{i}\,\gamma I_m - A)^{-1} \, \mathrm{d}\,\gamma. \tag{23}$$

This coincides with the standard observability Gramian for LTI systems, establishing that the time-averaged frequential formulation generalizes the classical result. ■

IV. Greedy Sensor Selection

This section introduces key concepts from submodular optimization theory and analyzes submodularity properties of common energy metrics. We present a greedy algorithm for sensor selection with guaranteed optimality bounds.

A. Supermodular and Non-Supermodular Set Functions

Definition 1 (Supermodularity): Let $\mathbb{N}_m$ be a finite ground set and $\rho : 2^{\mathbb{N}_m} \to \mathbb{R}$ be a set function. Function ρ is supermodular if for all $\mathcal{J}_1 \subseteq \mathcal{J}_2 \subseteq \mathbb{N}_m$ and $s \in \mathbb{N}_m \setminus \mathcal{J}_2$, we have

$$\rho(\mathcal{J}_1) - \rho(\mathcal{J}_1 \cup \{s\}) \geq \rho(\mathcal{J}_2) - \rho(\mathcal{J}_2 \cup \{s\}). \tag{24}$$

Definition 2 (Non-Increasing Set Function): A set function $\rho : 2^{\mathbb{N}_m} \to \mathbb{R}$ is said to be non-increasing if for all $\mathcal{J}_1, \mathcal{J}_2 \subseteq \mathbb{N}_m$ and $\mathcal{J}_1 \subseteq \mathcal{J}_2$, one has $\rho(\mathcal{J}_1) \geq \rho(\mathcal{J}_2)$.

We provide two key theorems on the supermodularity of two established metrics.

Theorem 1: Let $\Lambda_{\mathcal{J}}$ be the time-averaged frequential Gramian as defined in (11), with $\mathcal{J} \subseteq \mathbb{N}_m$. The set function

$$\rho(\mathcal{J}) = \log\det\left(\Lambda_{\mathcal{J}} + \varepsilon I_m\right)^{-1}\Big) \tag{25}$$

is supermodular and non-increasing.

Proof: From Lemma 1, $\Lambda_{\mathcal{J}}$ is well-defined, positive semi-definite (with $\Lambda_{\mathcal{J}} + \varepsilon I_m$ positive definite) and satisfies the additivity property. Following similar steps to those in

Algorithm 1 Frequency-Domain Greedy Sensor Placement

Input: constant K, parameter ε, matrix $\mathbf{T}$, and function $\rho \in \{\mathrm{tr}(\widehat{\Lambda}^{-1}),\ \log\det(\widehat{\Lambda}^{-1})\},\ \widehat{\Lambda} = \tilde{\Lambda}_{\mathcal{J}} + \varepsilon I_m$.
Output: set of sensors $\mathcal{J} \subseteq \mathbb{N}_m$ with $\rho(\mathcal{J}) \leq K$.

1: $\mathcal{J} \leftarrow \emptyset$ and $\tilde{\Lambda}_{\mathcal{J}} \leftarrow \mathbf{0}_{m\times m}$
2: $\mathbf{T} \leftarrow$ compute $\mathbf{T} \in \mathbb{R}^{(2r+1)m\times(2r+1)m}$ according to (9)
3: **while** $\rho(\mathcal{J}) > K$ **do**
4: **for** $s \in \mathbb{N}_m \setminus \mathcal{J}$
5: **for** $\alpha_l \in [0, \omega/2]$, with $l \in \{1, \ldots, L\}$ **do**
6: **for** $\ell \in \{-r, \ldots, 0, \ldots, r\}$ **do**
7: $\Psi^{(\ell)}_{\mathcal{J},\alpha_l} \leftarrow$ solve $(\mathrm{i}\,\alpha_l I_m - \mathbf{T})^{\mathsf{H}}\, \Psi^{(\ell)}_{\mathcal{J},\alpha_l} = \mathbf{C}^{(\ell)}_s$ (18)
8: **if** $\gamma_l = \alpha_l + c\omega \geq 0$
9: $|\Psi_{\gamma_l}| \leftarrow$ store $\sum_{k=-r}^{r} \widehat{\Psi}_k(\gamma_l, \mathcal{J})\widehat{\Psi}_k(\gamma_l, \mathcal{J})^{\mathsf{H}}$
10: **end if**
11: **end for**
12: **end for**
13: $\tilde{\Lambda}_{\mathcal{J}\cup\{s\}} \leftarrow \tilde{\Lambda}_{\mathcal{J}} + 1/\pi \sum_{\gamma_l} \xi_l \beta_l |\Psi_{\gamma_l}|$ (15)
14: **end for**
15: $s^* \leftarrow \arg\max_{s\in\mathbb{N}_m\setminus\mathcal{J}} \{\rho(\mathcal{J}) - \rho(\mathcal{J}\cup\{s\})\}$
16: $\mathcal{J} \leftarrow \mathcal{J}\cup\{s^*\}$ and $\tilde{\Lambda}_{\mathcal{J}} \leftarrow \tilde{\Lambda}_{\mathcal{J}\cup\{s^*\}}$
17: **end while**

[16, Proposition 2], we have that (25) is a supermodular and non-increasing set function. ■

Remark 2: Let $\tilde{\Lambda}_{\mathcal{J}}$ denote the first term in the right-hand side of (15), i.e., the approximate time-averaged frequential Gramian. One can verify that $\tilde{\Lambda}_{\mathcal{J}}$ is well-defined, positive semi-definite, and additive using similar arguments as in the proof of Lemma 1. In (25), we can alternatively use $\tilde{\Lambda}_{\mathcal{J}}$. The supermodularity of the resulting set function can be shown following the same steps as in the proof of Theorem 1.

Proposition 3: Let $\Lambda_{\mathcal{J}}$ be the time-averaged frequential Gramian as defined in (11), with $\mathcal{J} \subseteq \mathbb{N}_m$. The set function

$$\rho(\mathcal{J}) = \mathrm{tr}\Big(\big(\Lambda_{\mathcal{J}} + \varepsilon I_m\big)^{-1}\Big), \tag{26}$$

is non-supermodular.

Proof: Lemma 2 provides a case where the time-averaged frequential Gramian reduces to the standard observability Gramian. Following steps similar to those in [17], one can show by counterexample that (26) is not supermodular. ■

The regularization parameter ε in (25) and (26) guarantees the existence of well-defined solutions to $\rho(\mathcal{J})$ for arbitrary $\mathcal{J} \subseteq \mathbb{N}_m$, thereby eliminating the necessity of imposing observability a priori. Moreover, as $\varepsilon \to 0$, the regularized function approaches the original, unperturbed function [15], [16]. While the precise implications of the regularization parameter ε on observability properties in the context of frequential Gramians are less obvious, it nevertheless serves as an effective mechanism for ensuring invertibility of $\Lambda_{\mathcal{J}} + \varepsilon I_m$.

B. Greedy Algorithm

For the minimal sensor placement problem with bounded energy (6), the greedy algorithm presented in Algorithm 1 iteratively selects sensors that provide the maximum marginal improvement in the selected energy metric. Specifically, at each iteration, we select a sensor that maximizes the decrease in $\rho(\mathcal{J}) - \rho(\mathcal{J}\cup\{s\})$ for each sensor $s \in \mathbb{N}_m \setminus \mathcal{J}$. The algorithm iterates this process until termination, which is when the performance metric $\rho(\mathcal{J})$ meets the desired tolerance K.

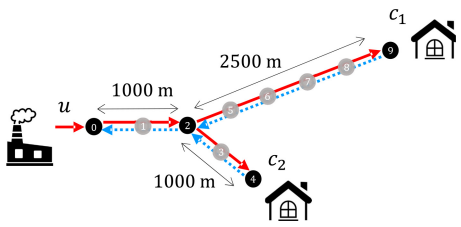

Fig. 1. District heating network topology in numerical experiments.

Proposition 4: The computational complexity of Algorithm 1 is $O(Lm^5(2r+1)^4)$, where m is the number of possible sensors, L is the number of samples over $[0, \omega/2]$, and $2r+1$ denotes the range of considered frequency modes.

Proof: The four nested loops in lines 3 to 6 contribute $O(m^2L(2r+1))$ iterations. The most intensive operation occurs at line 7, solving a linear system with a $(2r+1)m \times (2r+1)m$ matrix, requiring $O(m^3(2r+1)^3)$ operations per solution. Combining these factors yields a dominant complexity component of $O(Lm^5(2r+1)^4)$. ■

Remark 3: Supermodularity provides greedy algorithms such as Algorithm 1 with provable approximation guarantees similar to those established for the standard observability Gramian. For the function $\rho(\mathcal{J}) = \log\det((\Lambda_{\mathcal{J}} + \varepsilon I)^{-1})$, the solution to Algorithm 1 terminating at iteration k, i.e., $\mathcal{J}^{\mathrm{gr}} = \mathcal{J}_k$, satisfies

$$\begin{aligned}\frac{|\mathcal{J}_k|}{|\mathcal{J}^*|} &\leq 1 + \log\frac{\rho(\emptyset) - \rho(\mathbb{N}_m)}{\rho(\mathcal{J}_{k-1}) - \rho(\mathbb{N}_m)} \\ &\leq 1 + \log\frac{-m\log(\varepsilon) + \log\det\big(\Lambda_{\mathbb{N}_m} + \varepsilon I_m\big)}{K + \log\det\big(\Lambda_{\mathbb{N}_m} + \varepsilon I_m\big)},\end{aligned} \tag{27}$$

with respect to $\mathcal{J}^*$, the optimal solution to (6). The second inequality follows from the fact that $\rho(\mathcal{J}_{k-1}) > K$.

V. Numerical Experiments

We compare our frequential Gramian sensor placement against a standard approach using the observability Gramian with time-averaged dynamics. For fair comparison, we first execute Algorithm 1 until threshold K is reached, obtaining sensor configuration $\mathcal{J}_{\mathrm{freq}}$. Subsequently, we run Algorithm 1 with $\bar{A} = \frac{1}{T}\int_0^T A(\tau)d\tau$ until a configuration $\mathcal{J}_{\mathrm{sd}}$ with cardinality equal to $|\mathcal{J}_{\mathrm{freq}}|$ is found. For both methods, we employ the trace metric $\rho(\mathcal{J}) = \mathrm{tr}((\Lambda_{\mathcal{J}} + \varepsilon I_m)^{-1})$ with $\varepsilon = 10^{-5}$.

1) Experiment Setup: We consider the DHN depicted in Figure 1 with two topologies: (a) an open-loop configuration i.e., a non-cyclic network of 10 nodes from generation point to consumers, and (b) a closed configuration which additionally features return connections from consumers to generation point. System dynamics are modeled with $\omega = 0.001\pi$ rad/s, $\zeta_e = 0.01$, for any pipe e, and truncation parameters $r = 8$. Flow velocities follow a periodic pattern $v(t) = v_{\mathrm{sc}} \odot (\bar{v} + \alpha s(t))$, with $s(t) = \sin(2\omega(t-1)) + 0.7\sin(\frac{1}{2}\omega t)$, where $\odot$ represents element-wise multiplication, and the scaling factors are $v_{\mathrm{sc},i} = 1$ for $i \in \{0, 1, 2\}$, $v_{\mathrm{sc},i} = \lambda(t)$ for $i \in$

TABLE I
FREQUENCY-BASED VS. STANDARD SENSOR PLACEMENT

Parameters $(\overline{v}, \alpha, \overline{\lambda}, \beta)$	Sensors FB	Sensors SD	GIR	RMSE$\pm\sigma$ FB	RMSE$\pm\sigma$ SD	PIP (%)
			OL			
$(\frac{2}{5}, 0, \frac{1}{2}, \frac{1}{5})$	{9,4,2,6}	{9,4,5,1}	6.55	.133±.016	.144±.022	**7.6**
$(\frac{3}{5}, \frac{2}{5}, \frac{1}{4}, \frac{1}{10})$	{4,9,6,1}	{9,4,5,1}	2.13	.098±.026	.105±.028	**6.7**
$(\frac{3}{5}, \frac{2}{5}, \frac{1}{2}, \frac{7}{20})$	{9,4,6}	{9,4,5}	1.92	.127±.024	.130±.021	**2.3**
$(1, \frac{3}{5}, \frac{3}{4}, \frac{1}{10})$	{9,6,4,1}	{9,4,2,7}	20.95	.103±.017	.102±.014	**-1.0**
$(\frac{6}{5}, \frac{2}{5}, \frac{1}{2}, \frac{1}{10})$	{9,4,1,7}	{9,4,5,2}	2.70	.076±.006	.082±.007	**7.3**
$(\frac{6}{5}, 1, \frac{1}{2}, \frac{1}{5})$	{9,4,1,6}	{9,4,5,2}	2.77	.077±.015	.083±.017	**7.2**
			CL			
$(\frac{2}{5}, 0, \frac{1}{2}, \frac{1}{5})$	{4,7,0}	{4,9,5}	1.48	.160±.023	.164±.028	**2.4**
$(\frac{3}{5}, \frac{2}{5}, \frac{1}{4}, \frac{1}{10})$	{4,6,0}	{3,9,6}	0.98	.112±.032	.111±.034	**-0.9**
$(\frac{3}{5}, \frac{2}{5}, \frac{1}{2}, \frac{7}{20})$	{1,7,4}	{4,9,2}	7.95	.128±.020	.139±.025	**7.9**
$(1, \frac{3}{5}, \frac{3}{4}, \frac{1}{10})$	{9,6,4}	{4,9,2}	1.85	.108±.013	.132±.022	**18.2**
$(\frac{6}{5}, \frac{2}{5}, \frac{1}{2}, \frac{1}{10})$	{4,6,1,9}	{4,9,5,1}	7.53	.076±.007	.082±.008	**7.3**
$(\frac{6}{5}, 1, \frac{1}{2}, \frac{1}{5})$	{4,6,1}	{4,9,2}	2.51	.093±.023	.096±.021	**3.1**

Note: σ=Standard deviation; OL=Open-Loop, CL=Closed-Loop; FB=Frequency-based; SD=Standard.

$\{3, 4\}$, and $v_{\text{sc},i} = 1 - \lambda(t)$ for $i \geq 5$, with scaling factors controlled by distribution parameter $\lambda(t) = \overline{\lambda} + \beta \sin(\frac{\pi t}{500})$. We conduct Monte Carlo simulations with 100 trials across several parameter sets denoted by $(\overline{v}, \alpha, \overline{\lambda}, \beta)$.

2) Performance Evaluation: In each trial, we implement a standard Kalman filter for each sensor configuration starting at a randomized $t_0 \sim \mathcal{U}(0, T)$ and $x_{\text{true}}(t_0) \sim \mathcal{N}(0, I_m)$ to capture as much as possible the variation in the dynamics. We compute the root mean square error (RMSE) using

$$\text{RMSE}(t_k) = \left[\frac{1}{n}\sum_{i=1}^{n}\left(x_{\text{true},i}(t_k) - \hat{x}_{\text{KF},i}(t_k)\right)^2\right]^{\frac{1}{2}}. \quad (28)$$

Performance improvement percentage (PIP) is quantified as

$$\text{PIP}(\%) = 100 \cdot \frac{\text{MeanRMSE}_{\text{sd}} - \text{MeanRMSE}_{\text{freq}}}{\text{MeanRMSE}_{\text{sd}}}. \quad (29)$$

Furthermore, we compute the Gramian improvement ratio (GIR), i.e., the ratio between the frequential Gramians obtained from the frequency-based set $\mathcal{J}_{\text{freq}}$ and the set obtained using the standard metric $\mathcal{J}_{\text{sd}}$, which is defined as $\text{GIR} = \Lambda_{\mathcal{J}_{\text{sd}}} / \Lambda_{\mathcal{J}_{\text{freq}}}$. Results are shown in Table I.

3) Discussion: Our analysis comparing frequency-based and standard sensor placement methods shows the frequency-based approach demonstrated positive performance in five of six cases for both open-loop and closed-loop configurations, with PIPs ranging from -1.0% to 7.6% in open-loop and -0.9% to 18.2% in closed-loop. Higher mean velocities generally resulted in improvements exceeding 7%. Interestingly, Gramian ratio values did not reliably predict performance gains; the configuration with the highest ratio of 20.95 showed a performance decrease, while others with lower GIR values sometimes achieved significant improvements. These findings indicate that frequency-based sensor placement offers meaningful advantages over standard approaches, though benefits vary significantly with specific network configurations.

VI. CONCLUSION

We presented a novel frequency-domain framework for sensor placement in district heating networks using frequential Gramians to capture both periodic behaviors and slow thermal transients. We established key theoretical properties, including frequency mode decomposition that enables efficient computation. Our numerical experiments demonstrate that frequency-based sensor placement outperforms standard approaches with improvements of up to 18.2% in state estimation accuracy.

For future work, one may extend the developed methodologies to address uncertainties arising from demand variations. Furthermore, the arguments and discussion in this letter can be generalized to any systems with similar structure.

REFERENCES

[1] J. E. Machado, M. Cucuzzella, and J. M. Scherpen, "Modeling and passivity properties of multi-producer district heating systems," *Automatica*, vol. 142, Aug. 2022, Art. no. 110397.

[2] M. Sibeijn, S. Ahmed, M. Khosravi, and T. Keviczky, "Economic nonlinear model predictive control of Prosumer district heating networks," *IEEE Trans. Control Syst. Technol.*, early access, May 2, 2025, doi: 10.1109/TCST.2025.3561501.

[3] A. Benonysson, B. Bøhm, and H. F. Ravn, "Operational optimization in a district heating system," *Energy Convers. Manage.*, vol. 36, no. 5, pp. 297–314, 1995.

[4] M. Sibeijn, M. Khosravi, and T. Keviczky, "Mitigating short-sightedness of MPC for district heating networks using dual dynamic programming," in *Proc. IEEE Conf. Decis. Control (CDC)*, 2024, pp. 4608–4614.

[5] B. van der Heijde, "Optimal integration of thermal energy storage and conversion in fourth generation thermal networks," Ph.D. dissertation, Dept. Eng. Sci. Mech. Eng., KU Leuven, Leuven, Belgium, 2019.

[6] A. Matei, A. Bott, L. Rehlich, F. Steinke, and S. Ulbrich, "Optimal sensor placement in district heating networks for Bayesian inference of uncertain demands," in *Proc. UNCECOMP 4th Int. Conf. Uncertainty Quant. Comp. Sci. Eng.*, 2021, pp. 178–193.

[7] T. H. Summers and J. Lygeros, "Optimal sensor and actuator placement in complex dynamical networks," *IFAC Proc. Vol.*, vol. 47, no. 3, pp. 3784–3789, 2014.

[8] F. Pasqualetti, S. Zampieri, and F. Bullo, "Controllability metrics, limitations and algorithms for complex networks," *IEEE Trans. Control Netw. Syst.*, vol. 1, no. 1, pp. 40–52, Mar. 2014.

[9] K. Morris, "Linear-quadratic optimal actuator location," *IEEE Trans. Autom. Control*, vol. 56, no. 1, pp. 113–124, Jan. 2011.

[10] L. M. Dang et al., "Daily and seasonal heat usage patterns analysis in heat networks," *Sci. Rep.*, vol. 12, no. 1, p. 9165, 2022.

[11] A. J. Krener and K. Ide, "Measures of unobservability," in *Proc. IEEE Conf. Decis. Control (CDC)*, 2009, pp. 6401–6406.

[12] K. Manohar, B. W. Brunton, J. N. Kutz, and S. L. Brunton, "Data-driven sparse sensor placement for reconstruction: Demonstrating the benefits of exploiting known patterns," *IEEE Control Syst. Mag.*, vol. 38, no. 3, pp. 63–86, Jun. 2018.

[13] X. Wu, B. Jacob, and H. Elbern, "Optimal control and observation locations for time-varying systems on a finite-time horizon," *SIAM J. Control Optim.*, vol. 54, no. 1, pp. 291–316, 2016.

[14] A. Padovan and C. W. Rowley, "Continuous-time balanced truncation for time-periodic fluid flows using frequential Gramians," *J. Comput. Phys.*, vol. 496, Jan. 2024, Art. no. 112597.

[15] V. Tzoumas, M. A. Rahimian, G. J. Pappas, and A. Jadbabaie, "Minimal actuator placement with bounds on control effort," *IEEE Trans. Control Netw. Syst.*, vol. 3, no. 1, pp. 67–78, Mar. 2016.

[16] V. Tzoumas, M. A. Rahimian, G. J. Pappas, and A. Jadbabaie, "Minimal actuator placement with bounds on control effort," 2016, *arXiv:1409.3289*.

[17] T. H. Summers, F. L. Cortesi, and J. Lygeros, "Corrections to 'on submodularity and controllability in complex dynamical networks,'" *IEEE Trans. Control Netw. Syst.*, vol. 5, no. 3, p. 1503, Sep. 2018.